





Cite this: *Polym. Chem.*, 2025, **16**, 2851

# Innovative synthesis of PPC-P-co-PLA multi-block copolymers *via* one-pot copolymerization and transesterification catalysed by alkyl boron and diverse Lewis bases†

Mei Meng,<sup>a,b</sup> Min Xiao,<sup>b</sup> Jintao Wang,<sup>a</sup> Peiyuan Li,<sup>a</sup> Xianli Wu <sup>\*a</sup> and Yuezhong Meng <sup>\*a,b,c</sup>

Carbon dioxide (CO<sub>2</sub>) has been utilized for synthesizing biodegradable polymers to promote sustainable energy conservation and mitigate emissions. Nonetheless, the low glass transition temperature of amorphous CO<sub>2</sub>-based polyester–polycarbonate (PPC-P) significantly impedes its practical application. Herein, semi-crystalline copolymers, PPC-P-co-PLA, were successfully synthesized *via* copolymerization of propylene oxide (PO), phthalic anhydride (PA), and CO<sub>2</sub> in combination with PLA through transesterification catalysed by Lewis acid–base pairs in a one-pot/one-step method. Metal-free catalysts were utilized for the first time to catalyse both ring-opening copolymerization and transesterification reactions for copolymer synthesis. The mechanism study of PLA transesterification catalysed by triethyl borane (TEB)/Lewis bases revealed that effective depolymerization and transesterification of PLA hinge on  $\alpha$ -H chemical shift alterations induced by the Lewis bases. Lewis acid–base pairs facilitate the formation of PPC-P-co-PLA multi-block copolymers by terminating one end of PPC-P with PLA segments *via* continuous transesterification reactions. Compared to PPC-P, the copolymers exhibit an increase in glass transition temperature by 5–7 °C and an elevation in thermal decomposition temperature by 18–45 °C. The optimal mechanical and rheological properties of PPC-P-co-PLA multi-block copolymers are achieved at a PLA concentration of 8 wt%. This study opens new avenues for the synthesis of semi-crystalline polyester–polycarbonate-based copolymers with high glass transition temperatures, thereby enriching the theoretical foundation for the synthesis of block copolymers.

Received 17th March 2025,  
Accepted 18th May 2025

DOI: 10.1039/d5py00272a

rsc.li/polymers

## 1. Introduction

Employing carbon dioxide (CO<sub>2</sub>) as a raw material for the synthesis of biodegradable polymers promotes energy savings, reduces emissions, and effectively addresses environmental concerns arising from single-use plastics.<sup>1–4</sup> The utilization of CO<sub>2</sub>-based biodegradable polyesters and polycarbonates as raw materials for the preparation of eco-friendly polymers has proven to be a highly effective and promising strategy, particularly following the seminal work on alternating copolymerization of CO<sub>2</sub> and epoxides to produce polycarbonates, pub-

lished in 1969.<sup>5</sup> Considerable research has been conducted to enhance the selectivity and productivity of polycarbonate synthesis. Various catalytic systems have been investigated, including metal complex catalysts, organic base cocatalysts and metal-free catalysts. Many metal complex catalysts are employed in ring-opening copolymerization (ROCOP) of epoxides and CO<sub>2</sub> such as zinc-based composites<sup>5–9</sup> and Zn–Co double metal cyanide complexes.<sup>10,11</sup> Homogeneous catalytic systems mainly consist of metal complexes and often necessitate the inclusion of organic bases, such as ammonium salts and amines, as cocatalysts.<sup>12–15</sup> Metal-free catalysts based on alkyl boron are undergoing rapid development, enabling their complete removal in acidified ethanol to produce non-toxic, colorless polycarbonates without the necessity for multistep catalyst/ligand synthesis.<sup>16–21</sup> Furthermore, diverse monomers, such as epoxides, anhydrides, and lactones, have been used to synthesize polycarbonates and their copolymers with enhanced properties, ultimately broadening their potential applications.<sup>22–25</sup> For instance, the ROCOP of propylene oxide (PO), phthalic anhydride (PA) and CO<sub>2</sub> led to the synthesis of polyester–polycarbonate (PPC-P) exhibiting exceptional

<sup>a</sup>College of Chemistry, Zhengzhou University, Zhengzhou 450001, China.  
E-mail: wuxianli@zzu.edu.cn, mengyzh@mail.sysu.edu.cn

<sup>b</sup>The Key Laboratory of Low-carbon Chemistry & Energy Conservation of Guangdong Province/State Key Laboratory of Optoelectronic Materials and Technologies, School of Materials Science and Engineering, Sun Yat-sen University, Guangzhou 510275, China

<sup>c</sup>Institute of Chemistry, Henan Academy of Sciences, Zhengzhou 450000, China

† Electronic supplementary information (ESI) available. See DOI: <https://doi.org/10.1039/d5py00272a>

strength and thermal stability.<sup>26,27</sup> This was attributed to the Lewis acid–base pairs formed through the coordination of chloride ( $\text{Cl}^-$ ) to boron. PPC-P exhibits excellent performance and biodegradability, with a degradation rate surpassing that of PBAT in a  $58 \pm 2$  °C composting test.<sup>26</sup> The glass transition temperature of 41 °C (PE 27%) makes PPC-P susceptible to deformation during transportation under high-temperature conditions, thereby limiting its potential applications. Incorporating semi-crystalline polymers to PPC-P could improve its thermal stability and performance.

Poly(lactide) (PLA), also referred to as poly(lactic acid), is a biodegradable, semi-crystalline polyester derived from renewable resources. It exhibits high strength, transparency, and non-toxicity. PLA exhibits biodegradability and disintegration under actual composting conditions, with minimal impact on the composting process.<sup>28</sup> PLA has found widespread applications in various fields, including packaging, disposable straws, textiles, biomedicine, and architecture.<sup>29</sup> Copolymerization is a key technique for synthesizing high-performance polymers. Several kinds of copolymers incorporating PLA segments have been synthesized through the ROCOP process using lactide, a subtype of lactone, as the feedstock.<sup>30–32</sup> Lactide also serves as a common monomer for synthesizing  $\text{CO}_2$ -based copolymers, which results in semi-crystalline degradable polymers and enhances the thermal properties of  $\text{CO}_2$ -based polycarbonates.<sup>33–35</sup> Both metal-based and metal-free catalysts have been attempted for the preparation of polycarbonates and PLA copolymers *via* copolymerization of lactide,  $\text{CO}_2$  and epoxides, such as PO,<sup>33,34</sup> cyclohexene oxide,<sup>36</sup> and citronellyl glycidyl ether.<sup>35</sup> A semicrystalline copolymer of poly(propylene carbonate) (PPC) and poly(L-lactide) (PLLA) with a high molecular weight ( $M_n$  127.0 kg  $\text{mol}^{-1}$ ) was synthesized *via* simultaneous feeding of PO and L-lactide utilizing zinc adipate as the catalyst.<sup>37</sup> A crystallization melting peak was observed in the PPC-*co*-PLLA copolymer when the molar content of lactide exceeded 12%, with a melting temperature ( $T_m$ ) of 164.5 °C. The highest molecular weight PPC-*co*-PLLA copolymer reported to date ( $M_n$  698.0 kg  $\text{mol}^{-1}$ ) was synthesized using a heterogeneous ternary catalyst system comprising SalenCoIII, zinc glutarate and PPNCl.<sup>38</sup> The catalyst system exhibited intermolecular collaboration between cobalt and zinc, resulting in enhanced catalytic activity. Metal-free catalysts, comprised of Lewis acid–base pairs formed by triethylboron (TEB) and Lewis bases, facilitated the ROCOP of PO,  $\text{CO}_2$  and lactide. A one-pot/one-step strategy was employed using these catalysts to prepare low-molecular-weight PPCLAS ( $M_n < 15$  kg  $\text{mol}^{-1}$ ). In the synthesis of PLA copolymers through ROCOP of lactide, PLA transesterification acts as a side reaction that considerably affects the molecular weight of the resultant copolymer. Meanwhile, a one-pot/two-step strategy was utilized, involving the initial synthesis of PPC followed by the addition of lactide to form PLA chains, yielding high-molecular-weight PLA-*co*-PPC ( $M_n$  46.5 kg  $\text{mol}^{-1}$ ).<sup>34</sup> Triblock copolymers of PLA-*b*-PPC-*b*-PLA can be synthesized using TEB and difunctional initiators, exhibiting a transition from brittle to ductile to elastomeric properties. The synthesis process

involves the initial preparation of PPC, followed by the addition of lactide to form PLA segments, with diphenylurea serving as a hydrogen-bonding activator.<sup>33</sup> The incorporation of high-strength semi-crystalline PLA copolymers offers dual advantages: preserving the benefits of PPC-P while enabling the creation of novel semi-crystalline copolymers.

Block copolymers can be synthesized *via* a transesterification approach. PLA-PCL-PLA triblock copolymers were synthesized using a sequential transesterification process. Specifically, a macroinitiator HO-PCL-OH, terminated with  $\alpha,\omega$ -hydroxyl groups, was first obtained from PCL. This macroinitiator then underwent transesterification with PLA in the presence of 1,5,7-triazabicyclo[4.4.0]dec-5-ene (TBD) and diols.<sup>39</sup> The transesterification is primarily governed by the interaction between alcohols and carboxyl groups, with diols<sup>39</sup> or triols<sup>40</sup> as the transesterification reagent. Catalysed by appropriate agents, the ester groups in polyesters and polyols facilitate the cleavage of polyester chains, resulting in the formation of hydroxyl-terminated polyesters. These intermediates then undergo further reactions with additional polyesters, ultimately resulting in the formation of block copolymers through transesterification. Our study demonstrates, for the first time, the successful transesterification of PLA without the need for additional diols, marking a significant advancement in the transesterification process of polyester materials.

Semi-crystalline PPC-P-*co*-PLA multi-block copolymers were successfully synthesized *via* transesterification, leveraging commercial high-modulus PLA as the raw material. The inclusion of PLA markedly enhanced the thermal properties of the material with 18–45 °C higher decomposition temperature than that of PPC-P. The one-pot/one-step approach was utilized to carry out ROCOP of PO, PA and  $\text{CO}_2$  in conjunction with the transesterification of PLA (ROCOP-T), wherein the reactants were simultaneously fed into the reaction system utilizing metal-free catalysts. The successful synthesis of PPC-P-*co*-PLA multiblock copolymers requires a balance between the copolymerization reaction rate and the rates of PLA depolymerization and transesterification. Multiple factors can affect the initiation of ROCOP-T, including the selection of Lewis acid–base pairs, ion porosity, deprotonation processes, and solvent effects. In this study, we investigated the transesterification reaction mechanism of ester groups catalysed by metal-free organic catalysts, with a focus on the open-loop processes involved in PLA chemical recycling. Specifically, we emphasized the partial depolymerization of PLA and its subsequent incorporation into PPC-P-*co*-PLA copolymers, rather than its conversion to LA. Utilizing PLA transesterification for copolymer preparation has important implications for the reuse and recycling of PLA, offering novel insights into polyester recycling and utilization.

## 2. Experimental materials and methods

### 2.1 Materials

Poly(lactide) (PLA; Macklin, ~80 000 Da) was dried at 80 °C for 96 hours in a blast air oven. Propylene oxide (PO; Energy, 99%)

was stirred and refluxed for 24 h over CaH<sub>2</sub> and then distilled at constant pressure prior to use. 1,8-Diazabicyclo[5.4.0]undec-7-ene (DBU; TCI, 98%) was stirred and refluxed for 24 h over CaH<sub>2</sub> and then distilled by reduced-pressure distillation. High-purity CO<sub>2</sub> (Guangqi Gas Co. Ltd, Guangzhou, China, >99.9999%), triethyl borane (TEB; Energy, 1 M in THF), bis(triphenylphosphine)iminium chloride (PPNCl; Alfa, 97%), triethylamine (TEA; Aladdin, ≥99.5%), benzyl alcohol (BnOH; TCI, 98%), 1,4-benzenedimethanol (BDM; Aladdin, 99%), 1,5,7-triazabicyclo[4.4.0]dec-5-ene (TBD; J&K, 98%), dicyclohexylurea (U1; TCI, >98%), 4-dimethyl aminopyridine (DMAP; Alfa, 99%), benzyl triethyl ammonium chloride (TEBAC; TCI, 98%), tetrapropyl ammonium chloride (TPACl; J&K, >97%), tetrabutyl ammonium chloride (TBACl; Alfa, 97%), tetraamyl ammonium chloride (TPNAC; TCI, >98%), tetrabutyl ammonium bromide (TEABr; J&K, 99%), tetrabutyl phosphonium chloride (TBPC; Macklin, 96%), benzyl triphenyl phosphonium chloride (BPP; TCI, >98%) and tetraphenylphosphonium chloride (TPPP; J&K, 98.5%) were used as received.

## 2.2 Characterization

<sup>1</sup>H NMR and <sup>13</sup>C NMR spectroscopy and diffusion-ordered NMR spectroscopy (DOSY) of PPC-P-co-PLA copolymers in deuterated chloroform (CDCl<sub>3</sub>) were performed on a Bruker DRX-400 MHz NMR spectrometer with tetramethylsilane (TMS) as an internal reference. Molecular weights were determined by Waters gel permeation chromatography (GPC) using tetrahydrofuran (THF) as the eluent (1 mL min<sup>-1</sup> at 40 °C) and polystyrene (PS) as the standard. Fourier transform infrared spectroscopy (FT-IR) was conducted using a PerkinElmer Spectrum 100 system within the wavelength range of 4000 cm<sup>-1</sup> to 500 cm<sup>-1</sup>. To enhance the visualization of variations in functional groups, we focused on the specific wavelength range of 2000 cm<sup>-1</sup> to 500 cm<sup>-1</sup>.

Thermogravimetric analysis (TGA) was performed using a PerkinElmer Pyris Diamond TG/DTA analyser under a nitrogen atmosphere (200 mL min<sup>-1</sup>) at a heating rate of 10 °C min<sup>-1</sup> in the temperature range of 30 to 650 °C. Differential scanning calorimetry (DSC) measurements were carried out on a DSC Model 204 (Netzsch) under nitrogen. The samples (around 5–10 mg) were first heated at a heating rate of 10 °C min<sup>-1</sup> from room temperature to 200 °C and then cooled at a cooling rate of 10 °C min<sup>-1</sup> to -30 °C using liquid nitrogen, followed by a second heating at a heating rate of 10 °C min<sup>-1</sup> in the temperature range of -30 to 200 °C. The crystalline melting temperature (*T*<sub>m</sub>) was measured from the first heating cycle. The glass transition temperature (*T*<sub>g</sub>) was measured from the second heating cycle. An X-ray diffractometer (XRD) model D/Max-III A, manufactured by Rigaku in Japan, was utilized to assess the crystallinity of the resulting polymer. This assessment employed Cu-Kα radiation, scanning at a rate of 1° min<sup>-1</sup> within a 2θ range spanning from 5° to 40°.

Mechanical properties were assessed using a computer-controlled Instron tester (Model 5566) at 25 °C and 50% ± 5% relative humidity, conforming to the ASTM E104 standard. Each sample was tested using five dumbbell-shaped specimens

measuring 25 mm × 4 mm × 1 mm, with average results reported. The stretching rate was set to 50 mm min<sup>-1</sup>. The rheological properties were characterized using a rotational rheometer (Haake MARS III, Thermo Fisher Scientific). Circular specimens, 1 mm thick and 25 mm in diameter, were prepared for rheological testing. The test parameters comprised a frequency range of 0.1–100 rad s<sup>-1</sup>, an amplitude of 1%, and a temperature of 170 °C.

## 2.3 The effect of PPNCl on PLA depolymerization

PLA (10 wt% or 5 wt%) and PPNCl were dissolved in PO at ratios ranging from 4000 : 1 to 200 : 1 (PO : PPNCl). The solution was then heated to 70 °C, cooled to room temperature, and subsequently analysed by <sup>1</sup>H NMR and GPC.

## 2.4 The effect of initiators on PLA transesterification

**2.4.1 PO/PLA/LB + TEB.** PLA (10 wt%) was dissolved in PO solution, followed by the addition of LB. The solution was heated at 70 °C for 2 hours, then cooled to room temperature, and analysed by <sup>1</sup>H NMR. Subsequently, TEB was added to the solution in a 4000 : 2 : 1 ratio of PO : TEB : LB. The mixture was heated at 70 °C for 2 hours, cooled, and then re-analysed by <sup>1</sup>H NMR.

**2.4.2 PO/PLA/TEB/LB.** PLA (10 wt%) was dissolved in PO solution, with LB and TEB added in a ratio of 4000 : 2 : 1 (PO : TEB : LB). <sup>1</sup>H NMR spectra were analysed after heating the solution at 70 °C for 2 hours.

## 2.5 Initiator activity for both PO/PA/CO<sub>2</sub> copolymerization and PLA transesterification

PLA/PO homogeneous solution was prepared by heating 1.1 g of PLA in 12.6 g of PO at 70 °C for 1 hour, followed by cooling to room temperature. Within the glove box, PO, PA, TEB, and LB in a ratio of 4000 : 500 : 2 : 1 (PO : PA : TEB : LB) and the PLA homogeneous solution were rapidly introduced into a dry reactor, which was then sealed tightly. The reactor was removed from the glove box and placed in a fume hood. Throughout the heating reaction at 65 °C, the CO<sub>2</sub> pressure was maintained below 1 Megapascal. After continuous copolymerization and PLA transesterification, the reactor was cooled to room temperature, allowing CO<sub>2</sub> to be released. A small aliquot of the mixture was then sampled for <sup>1</sup>H NMR analysis. The crude product was dissolved in CH<sub>2</sub>Cl<sub>2</sub>, and the reaction was quenched using a 1 mol L<sup>-1</sup> hydrochloric acid/ethanol solution. The polymer solution was precipitated by adding an 8-fold excess of ethanol. The product was dried in a blast drying oven at 60 °C for 24 hours, followed by vacuum drying at 80 °C for an additional 24 hours until constant weight was achieved. The mass of the weighed product is *m*<sub>product</sub>.

## 2.6 One-pot one-step synthesis of PPC-P-co-PLA

The specific reaction ratios utilizing PPNCl as the Lewis base are presented in Table 3. As detailed in entry 19 of Table 3, the crucial steps involved in synthesizing the copolymers are outlined below: A PLA/PO homogeneous solution was prepared by heating 2.2 g of PLA in 12.6 g of PO at 70 °C for 1 hour, and

then cooled to room temperature. Inside the glove box, 108  $\mu\text{L}$  of TEB, 31.2 mg of PPNCl, 4 g of PA, and the PLA/PO homogeneous solution were quickly transferred into a 50 ml reactor, which was then tightly sealed. The reactor was then removed from the glove box and placed in a fume hood. During the heating reaction at 65  $^{\circ}\text{C}$ , the  $\text{CO}_2$  pressure was maintained at 1 MPa. After washing and drying, the  $^1\text{H}$  NMR spectra,  $^{13}\text{C}$  NMR spectra, GPC, and FT-IR spectrum were analysed.

### 2.7 Geometric structure optimization calculation methods

The geometries of organic bases (TPACl, TBACl, TPNAC, TBPC, and TBABr) interacting with PLA chain segments were optimized with the M06-2X density functional and the 6-21G basis set using Gaussian.<sup>41</sup> To streamline the calculations, we focused solely on the impact of Lewis bases on a single PLA chain segment. Following the structural optimization of the TBACl-PLA interaction, the structural optimization calculation for the interaction between Lewis bases and PLA, including TBABr, TBPC, TPACl and TPNCl was conducted subsequently. The SMD implicit solvation model was used to evaluate the effect of PO as the solvent ( $\epsilon_{\text{ps}} = 16$ ,  $\epsilon_{\text{psinf}} = 1.9$ ) on the distance between ion pairs, taking into account the solvation effect of PO. The carbon atom carrying the  $\alpha\text{-H}$  of PLA exhibits stereoisomerism. To investigate the impact of stereoisomerism, we altered the positions of hydrogen and methyl groups on a specific carbon atom to optimize the geometry of PLLA (*S,S*) in complex with TBACl.

## 3. Results and discussion

### 3.1 Mechanism of PLA depolymerization and transesterification by metal-free catalysts

**3.1.1 Depolymerization of PLA.** To investigate the mechanism of PLA transesterification catalysed by TEB/Lewis bases (LB), a series of experiments were conducted involving PO, PLA, PPNCl and TEB. PPNCl, a widely employed Lewis base, is known for its application in the ROCOP of lactide, carbon dioxide and epoxides.<sup>34,42-44</sup> Initially, the interactions between the sole addition of a Lewis base and PLA using PPNCl as the initiator and PO as the solvent were examined. The reaction comprises two steps: initially, the nucleophilic reagent undergoes addition to the carbonyl carbon, forming a negatively charged tetrahedral intermediate. Subsequently, a negative ion is eliminated, resulting in the substitution reaction (Fig. 1a). The addition of PO and PPNCl induces a chemical shift of the tertiary hydrogen of PLA ( $\alpha\text{-H}$ ,  $\delta_{5.13-5.27}$ ) towards the right ( $\delta_{5.05-5.12}$ ) in the hydrogen spectrum. Once the initiator is fully integrated with PLA, the integral area of hydrogen undergoing a chemical shift does not exhibit an increase in proportion with reaction time (Fig. S1-S7<sup>†</sup>). It maintains a constant proportion relative to  $\alpha\text{-H}$  hydrogen atoms that remains unaffected by the chemical shift. This ratio exhibits an increase with the increase in the quantity of the initiator (Fig. 1b). GPC curves reveal a continuous decline in the molecular weight of the product with an increase in initiator

content, indicating stronger depolymerization of PLA (Fig. 1c) at higher ratios of initiators.

In the presence of THF as a solvent, the addition of a Lewis base can also induce the depolymerization of PLA. The degree of PLA depolymerization is enhanced upon the addition of PO (Fig. S8<sup>†</sup>). The chemical shift ( $\delta_{5.05-5.12}$ ) of hydrogen is observed exclusively with PO as the solvent, indicating that the interaction between PO and PPNCl preceded its action on PLA (Fig. S9b-e<sup>†</sup>). PLA depolymerization occurs through a nucleophilic substitution reaction under alkaline catalytic conditions. An incremental increase in PPNCl addition positively correlates with the proportion of rightward-shifted  $\alpha\text{-H}$ , suggesting that the observed chemical shift variations are not attributable to PLA decomposition into lactide ( $\delta_{5.06-5.14}$ , Fig. S6 and S14g, h<sup>†</sup>) but rather result from interactions between the initiator and PLA (Fig. 1a and b). These interactions subsequently alter the chemical environment surrounding proximal hydrogen atoms. Over time, the molecular weights of the depolymerized ester exchange products decrease slightly. The peak shape in the GPC curves remained constant (Fig. S10<sup>†</sup>). The incorporation of a Lewis base and PO initiates the depolymerization of PLA. The length of depolymerized PLA segments is intimately linked to the quantity of the Lewis base. Subsequently, the newly formed anions are less likely to attack PLA segments further. This observation supports the subsequent use of PLA transesterification, a displacement reaction, for the preparation of copolymers.

**3.1.2 Displacement reaction catalysed by alkyl boron.** The primary cause of PLA depolymerization is the addition of Lewis bases, whereas copolymer formation is attributed to the introduction of TEB. After adding TEB, the  $\alpha\text{-H}$  peak ( $\delta_{5.05-5.12}$ ) changes from four distinct peaks to a bulge in the  $^1\text{H}$  NMR spectra (Fig. S11a<sup>†</sup>). Post-integration with TEB, further analysis of the hydrogen spectrum reveals that the  $\alpha\text{-H}$  undergoing the chemical shift is associated with the moiety connected to  $\text{PPN}^+$ . PPO ( $\delta_{3.26-3.70}$ ) is synthesized by integrating PO with Lewis acid-base pairs, subsequently undergoing ring-opening polymerization of PO. The appearance of new peaks within the chemical shift range of 4.63–4.77 ppm and 3.83–4.43 ppm suggests interactions between PPO and PLA after adding TEB and PPNCl (Fig. S11a<sup>†</sup>). The incorporation of TEB enhances the generation of oxygen anions, whereas the addition of PO not only produces PPO but also initiates an interaction between PPO and PLA (Fig. S12a, e and f<sup>†</sup>). Upon the initial addition of TEB, a distinct peak at  $\delta_{4.46}$  was observed, accompanied by a complex peak structure involving  $-\text{CH}(\text{CH}_3)$  moieties around  $\delta_{3.96-4.21}$  (Fig. S11b<sup>†</sup>), indicating that a small amount of PLA can be activated *via* TEB.<sup>45</sup> A small amount of PPO is produced, with no significant chemical shift observed in the  $\alpha\text{-H}$  of PLA.

After adding PPNCl, there were no significant changes in the chemical shift or peak shape of the  $\alpha\text{-H}$  of PLA, but a large amount of PPO was produced. Our results suggest that TEB selectively binds to PO, and the addition of PPNCl initiates the ring-opening of PO, resulting in the formation of a substantial amount of PPO (Fig. S12b-d<sup>†</sup>). When TEB and PPNCl are com-



**Fig. 1** (a) Schematic diagram of PLA depolymerization using PPNCl as the initiator and PO as the solvent. ① Ionic Lewis bases engage in nucleophilic substitution reactions with PLA, resulting in the depolymerization of PLA. ② Ionic Lewis bases react with PO to form oxygen anions that exhibit a heightened propensity for nucleophilic substitution reactions with PLA, ultimately resulting in the depolymerization of PLA. <sup>1</sup>H NMR spectra (b) and GPC curves (c) of different concentrations of PPNCl and PLA by heating at 70 °C for 2 h. Naming conventions: the quantity of PO remains constant, while the value preceding PLA denotes its mass fraction; the notation 'nPPNCl' signifies the ratio of PO to PPNCl, where PO : PPNCl = 4000 : n. A<sub>5.13-5.23</sub> : A<sub>5.05-5.13</sub> represents the integral area ratio in the hydrogen spectrum.

bined, the GPC curves mimic those observed solely with PPNCl during the initial stage (0–1 h) (Fig. 2a). This implies that PLA depolymerization occurs in the initial reaction stage, facilitating copolymer synthesis in subsequent experiments. As the reaction progresses, the PPO content continues to increase (Fig. S13<sup>†</sup>). Following a 4-hour reaction, the depolymerization of PLA into various chain segment lengths was confirmed by the DOSY spectrum (Fig. 2b). Furthermore, the formation of PPO-*co*-PLA copolymers is apparent from the linkage between PPO and PLA (Fig. 2b and Fig. S12e, f<sup>†</sup>). The mere addition of a Lewis base promotes PLA depolymerization, whereas the inclusion of Lewis acid–base pairs enhances the formation of PPO-*co*-PLA copolymers through a displacement reaction.

**3.1.3 Interaction between TEB/LB and PLA.** Extensive experiments were conducted to investigate the transesterification mechanism of PLA using six distinct types of Lewis bases: organic amines (TEA), amidines (DBU and TBD), urea (U1), pyridine (DMAP), organic amine salts (TEBAC, TPACl, TBACl, TPNAC, and TBABr), and organic phosphine salts (TBPC, BPP, TTPP, and PPNCl) (Fig. 3a). These Lewis bases are frequently

utilized in the ring-opening polymerization of lactide or the ROCOP of PO and CO<sub>2</sub>.<sup>18,34,46</sup> The first four types are categorized as non-ionic initiators, whereas the remaining two types are classified as organic salts. The depolymerization of PLA occurs exclusively through nucleophilic substitution reactions involving Lewis bases, generating a terminus with an oxygen anion that initiates the ester exchange process within the PLA matrix. The rightward shift in the chemical shift caused by certain initiators (DBU, TEBAC, TPACl, TBACl, TPNCl, TBPC, BPP, TTPP and PPNCl) transitioned from distinct peaks (Fig. 3b) into a bulge with the incorporation of TEB (Fig. 3c) in <sup>1</sup>H NMR spectra. Interestingly, the incorporation of TEB led to the formation of PPC-*P-co*-PLA multi-block copolymers as products of copolymerization and transesterification reactions catalysed by the aforementioned initiators with the peak-shape of  $\alpha$ -H in PLA changed (Fig. 5). TEB plays a crucial role in the synthesis of copolymers through copolymerization and PLA transesterification, highlighting the importance of Lewis acids. TEB, as a metal-free Lewis acid, efficiently promotes transesterification under mild conditions by activating electrophilic



Fig. 2 (a) GPC curves of PO:TEB:PPNCl 4000:2:1, with PLA at 10 wt% at 70 °C over different times. (b) DOSY spectrum of PO:TEB:PPNCl 4000:2:1, with PLA at 10 wt% at 70 °C for 4 hours.

reagents and facilitating the formation of intermediates, which enhances the overall transesterification process (Fig. S12a†). The effective binding of TEB to the oxygen anion terminus of PLA during depolymerization is crucial for facilitating the formation of copolymers.

Upon the concurrent addition of TEB and Lewis base systems to the homogeneous PLA/PO solution, DBU and TBD, two specific initiators, induced a rightward shift in the chemical shift of  $\alpha$ -H in PLA (Fig. 3d). DBU binds to both oxygen anions and carbonyl groups of PLA *via* the alcohol activation pathway and nucleophilic attack pathway (Fig. S15†).<sup>47–50</sup> The incorporation of TEB mainly influences the  $\alpha$ -H in PLA positioned near oxygen anions, with minimal effect on the  $\alpha$ -H attached to the carbonyl group adjacent to DBU or TBD. The chemical shift in the partial  $\alpha$ -H of PLA, induced by DBU or TBD, is observable in Fig. 3b, 2c and d. Therefore, the mechanisms underlying PLA depolymerization and transesterification, initiated by ionic and non-ionic species, differ. During depolymerization, ionic Lewis bases aid in the splitting of PLA into two chains, which then associate with anions and cations, respectively. Non-ionic Lewis bases, exemplified by DBU, exhibit robust protonation and deprotonation capabilities, allowing them to interact with the carbonyl groups and oxygen anions of PLA after depolymerization.

By analyzing the hydrogen spectrum of  $\alpha$ -H in the PLA <sup>1</sup>H NMR spectra, preliminary predictions can be made regarding the potential occurrence of depolymerization and transesterification. Specific Lewis bases, including TEA, TEA/BnOH, and U1, do not induce a chemical shift towards the higher-frequency side of  $\alpha$ -H in PLA, nor do they initiate PLA transesterification when used as initiators. The results support this hypothesis. Using TEA and TEA/BnOH as initiators can solely initiate ROCOP of PO, PA and CO<sub>2</sub> to produce PPC-P/PLA blends without inducing PLA transesterification (Fig. 5b, Fig. S16† and Fig. 3e). U1, when used as an initiator, cannot initiate copolymerization or transesterification of PLA (Fig. 3e). Therefore, if a LB does not cause shifts in the chemical resonance of partial  $\alpha$ -H in PLA, it indicates that PLA depolymerization has not taken place, implying that transesterification of PLA is improbable.

**3.1.4 Distances of ion pairs and PLA.** The depolymerization and transesterification of PLA, as well as the ROCOP of PO, PA and CO<sub>2</sub> involve intricate interaction with anions, exhibiting a profound interdependence. Fundamentally, these reactions revolve around active centers, which include ion pairs and free ions, maintained in a delicate equilibrium. In this reactive environment, the dominant active centers consist of loosely bound ion pairs, which solvents effectively disperse and separate, thus facilitating the reaction progression. The degree of ion pair loosening significantly impacts ROCOP-T. Quantum chemistry methods were employed to measure the anion–cation distance, the distance between anions and PLA, and the bond lengths of adjacent PLA atoms (Fig. 4 and Table 1).<sup>41</sup> The data indicate that the chloride ions from TBACl exhibit a closer proximity to one of the  $\alpha$ -H positions in PLLA (*S,S*) conformations. Given the reduced steric hindrance of PLLA (*S,S*) compared to PLA (*R,S*), the anion is positioned closer to the ester group of PLLA (*S,S*) (Table 1f and m). This phenomenon is particularly evident when a single hydrogen atom is in close proximity to the anion. The optimized geometries of various Lewis bases and PLA (*R,S*) systems were analysed to investigate the effects of anions on  $\alpha$ -H interactions.

An increase in steric hindrance, such as TPACl, TBACl, and TPNCl, leads to a progressive increase in the distance between chloride ions and the positive charge center and a decrease of the hydrogen bond formed between anions and the  $\alpha$ -H of PLA (Table 1a and b). The difference in hydrogen bond distances between TBACl and TPNCl is negligible. Our experimental results align with the findings, suggesting that further elongation of LB's carbon chains is unlikely to yield beneficial outcomes in the synthesis of PPC-P-*co*-PLA multi-block copolymers (entries 10 and 11, Table 2). Ionic bonds are intrinsically related to the electrostatic attraction between anions and cations. Compared to TBACl, TBABr exhibits a larger distance between anions and cations, as well as weaker hydrogen bonding between anions and the  $\alpha$ -H of PLA, due to the larger atomic radius of Br compared to Cl (Table 1a and b). The shorter distance between the anion of TBABr and the carbonyl group indicates a positional shift of the anion (Table 1c and



**Fig. 3** (a) Schematic diagram of the structural formulas of Lewis bases and TEB. <sup>1</sup>H NMR spectra of (b) PO/PLA/LB at 70 °C for 2 h; (c) adding TEB into PO/PLA/LB at 70 °C for 2 h; (d) PO/PLA/TEB/LB at 70 °C for 2 h and (e) products resulting from the copolymerization of PO, PA, and CO<sub>2</sub> and PLA transesterification with TEB and different Lewis bases at 65 °C for 6 h.

d). The positional shift likely contributes to the weaker attraction of TBABr to the  $\alpha$ -H of PLA compared to TBACl, resulting in the absence of the ester exchange reaction. Substituting the nitrogen (N) in TBACl with phosphorus (P) results in a shortened distance between anions and cations, enhanced hydrogen bonding between anions and the  $\alpha$ -H of PLA, and increased distances between the anion and the carbonyl group in TBPC compared to TBACl. TBPC exhibits a stronger attraction to the  $\alpha$ -H of PLA than TBACl (Table 1 a–d). An enlargement of the cation radius leads to reduced separation between

anions and cations. Furthermore, this enlargement prompts anions to shift towards the  $\alpha$ -H region of PLA. The close proximity of anions in the initiator to the  $\alpha$ -H of PLA enhances transesterification, ultimately facilitating copolymer synthesis.

**3.1.5 Deprotonation of  $\alpha$ -hydrogen in PLA mediated by Lewis bases.** The formation of a lactide enolate through deprotonation by a strong Lewis base is crucial for the ring-opening polymerization of lactide to produce PLA.<sup>51,52</sup> This study also validated the interaction between L-lactide and organic Lewis bases by <sup>1</sup>H NMR spectroscopy (Fig. S14<sup>†</sup>). The employment of



**Fig. 4** M06-2X/6-21G optimized geometries of TBACl and the chain segment of (a) PLA (*R,S*) or (b) PLLA (*S,S*). M06-2X/6-21G optimized geometries of (c) PLA (*R,S*) and (d) PLA (*R,S*) affected by chloride ions in TBACl. To enhance the observation of structural alterations, the chain segment orientation of PLA (*R,S*) in (c) and (d) is reversed relative to that observed in (a).

**Table 1** Distance from anions to cations, anions to PLA and partial bond length of PLA obtained from optimized geometries<sup>a</sup>

Distance/Å	PLA	TPACl	TBACl	TPNCl	TBPC	TBABr	TBACl <sup>PO</sup>	PLLA	TBACl <sup>PLLA</sup>
a (anion...cation)	—	3.9283	3.9568	3.9660	3.8496	4.0442	4.2229	—	3.9522
b (anion...H)	—	2.5748	2.5412	2.5374	2.5384	2.6092	2.7309	—	2.6387
c (anion...O)	—	3.6462	3.7701	3.8265	3.8251	3.8044	3.6433	—	3.5382
d (anion...C)	—	3.3732	3.5052	3.5466	3.5486	3.5116	3.3978	—	3.1613
e (anion...O)	—	3.3313	3.3647	3.3589	3.4039	3.3701	3.3900	—	3.2350
f (C-H)	1.0934	1.0934	1.0937	1.0934	1.0937	1.0933	1.0948	1.0935	1.0948
g (C-O)	1.4208	1.4240	1.4238	1.4246	1.4255	1.4239	1.4311	1.4197	1.4222
h (O-C)	1.3518	1.3363	1.3355	1.3344	1.3363	1.3353	1.3364	1.3532	1.3393
i (C=O)	1.1998	1.2088	1.2083	1.2086	1.2078	1.2084	1.2096	1.1998	1.2085
j (C-C)	1.5176	1.5168	1.5148	1.5144	1.5159	1.5151	1.5169	1.5141	1.5122
k (O-C)	1.3492	1.3458	1.3482	1.3496	1.3471	1.3483	1.3458	1.3486	1.3479
l (O-C)	1.3386	1.3552	1.3544	1.3538	1.3537	1.3543	1.3316	1.3373	1.3549
m (C=O)	1.2024	1.2009	1.2007	1.2008	1.2010	1.2009	1.2112	1.2036	1.2008
n (C-C)	1.5249	1.5181	1.5166	1.5167	1.5168	1.5149	1.5188	1.5254	1.5184
m (anion...H)	—	—	—	—	—	—	—	—	2.9110

<sup>PO</sup>: the SMD implicit solvation model employed to assess the influence of PO as the solvent ( $\epsilon_{\text{ps}} = 16$ ,  $\epsilon_{\text{psinf}} = 1.9$ ). <sup>PLLA</sup>: M06-2X/6-21G optimized geometries of TBACl and the chain segment of PLLA (*S,S*). <sup>a</sup> The detailed data pertaining to the computational outcomes are presented in Data S1–S9.†

three Lewis bases – TBACl, TPNCl and PPNCl – facilitates the deprotonation leading to the formation of a lactide enolate. The deprotonation effect consistently persists throughout the interaction between Lewis bases and PLA as monitored using <sup>1</sup>H NMR spectra and M06-2X/6-21G optimized geometries.

Variations in the chemical environment of  $\alpha$ -H lead to discernible changes in the peak shape of PLA in the <sup>1</sup>H NMR spectra. The peak shape of  $\alpha$ -H in PLA became asymmetric with the addition of PPNCl and THF as the solvent (Fig. S9e†). Furthermore, as the content of the Lewis base increased, the

**Table 2** The effect of a Lewis base and TEB on the  $\alpha$ -H of PLA and product prediction and actual products by copolymerization of PO, PA, and CO<sub>2</sub> and PLA transesterification

Entry	Initiator	$\alpha$ -H chemical shift <sup>a</sup>		Product	$m_{\text{Product}}$ (g)	Yield <sup>b</sup> (%)	Conv. PE <sup>c</sup> (%)	PE <sup>c</sup> (%)	PPC <sup>c</sup> (%)	PPO <sup>c</sup> (%)	PLA <sup>c</sup> (%)	CO <sub>2</sub> <sup>c</sup> (wt%)	Selectivity <sup>c</sup> (%)	$M_n^d$ (kg mol <sup>-1</sup> )	PDI <sup>d</sup>
		2 h	+TEB2 h												
1	TEA	NO	NO	PPC-P/PLA blends	9.53	53.3	100	36.7	42.6	2.3	18.5	14.0	97.6	49.1	1.47
2	TEA/BnOH	NO	NO	PPC-P/PLA blends	7.24	42.3	100	52.2	27.0	1.4	19.4	7.89	97.6	28.8	1.50
3	DBU	YES	YES	PPC-P-co-PLA/PLA blends	8.17	43.4	100	35.8	44.0	0	20.3	14.5	100	24.6	1.38
4	TBD	YES	NO	PE-co-PLA	3.79	21.5	54.7	43.9	0	0.3	55.8	0	100	17.3	1.51
5	U1	NO	NO	—	1.10	—	0	0	0	0	100	0	0	—	—
6	DMAP	YES	NO	—	0.93	—	0	0	0	0	100	0	0	—	—
7	U1/DMAP/BDM	YES	NO	PE/PLA blends	1.12	—	19.2	14.9	0	1.6	83.5	0	—	—	—
8	TEBAC	YES	YES	PPC-P-co-PLA/PLA blends	9.95	52.1	100	34.4	42.9	3.0	19.7	14.5	90.9	33.8	1.46
9	TPACL	YES	YES	PPC-P-co-PLA	8.68	45.6	100	32.7	46.5	1.4	19.3	15.8	95.2	39.1	1.59
10	TBACl	YES	YES	PPC-P-co-PLA	11.7	59.7	100	31.7	48.6	1.2	18.6	16.6	96.2	53.7	1.42
11	TPNAC	YES	YES	PPC-P-co-PLA	10.3	53.1	100	30.1	49.1	2.5	18.3	17.0	95.2	58.2	1.37
12	TEABr	YES	NO	PPC-P/PLA blends	8.38	45.2	100	42.2	32.9	1.5	23.4	10.5	90.7	30.3	1.41
13	TBPC	YES	YES	PPC-P-co-PLA/PLA blends	7.82	42.5	91.4	43.3	29.8	0.9	26.0	9.41	98.2	39.8	1.54
14	BPP	YES	YES	PPC-P-co-PLA	11.7	58.5	100	25.3	55.6	3.3	15.8	20.0	95.7	46.5	1.36
15	TTPP	YES	YES	PPC-P-co-PLA	10.7	55.8	100	32.1	41.1	1.2	25.6	14.2	100	46.0	1.59
16	PPNCl	YES	YES	PPC-P-co-PLA	12.3	61.4	100	27.6	54.8	2.9	14.8	19.3	99.4	60.5	1.59

<sup>a</sup> The results are sourced from Fig. 3b and c. <sup>b</sup>  $m_{\text{reactant}} = 12.55 \text{ g (PO)} + 4.00 \text{ g (PA)} + 1.10 \text{ g (PLA)}$  and  $\text{CO}_2 \text{ wt\%} = m_{\text{Product}}/m_{\text{reactant}} \times 100$ ; blends: yield % =  $(m_{\text{Product}} - m_{\text{PLA}})/(m_{\text{reactant}} - m_{\text{PLA}}) \times 100$ ; PPC% =  $A_4/(A_1/4 + A_4 + (A_{6,7})/3 + A_8) \times 100$ ; PPO% =  $(A_{6,7})/3 + A_8 + (A_{6,7})/3 + A_8) \times 100$ ; PLA% =  $A_8/(A_1/4 + A_4 + (A_{6,7})/3 + A_8 + A_c) \times 100$ ; CC% =  $100 - \text{CO}_2\%$ ; selectivity% =  $100 - \text{CO}_2\%$ . <sup>c</sup> Calculated by <sup>1</sup>H NMR; PE% =  $A_4/(A_1/4 + A_4 + (A_{6,7})/3 + A_8) \times 100$ ; PPC% =  $A_4/(A_1/4 + A_4 + (A_{6,7})/3 + A_8) \times 100$ ; PPO% =  $(A_{6,7})/3 + A_8 + (A_{6,7})/3 + A_8) \times 100$ ; PLA% =  $A_8/(A_1/4 + A_4 + (A_{6,7})/3 + A_8 + A_c) \times 100$ . <sup>d</sup> Determined by GPC in tetrahydrofuran (THF).

peak shape changed significantly (Fig. S9†). Consequently, the peak shape is modified due to the proximity of the anion site to the  $\alpha$ -H side. Notably, the incorporation of anions exerts a contrasting influence on the bond lengths of the two ester groups linked to the carbon bearing an  $\alpha$ -H (Table 1h, 1l and Fig. 4c, d). The deprotonation of the  $\alpha$ -H of PLA by anions forms enolate intermediates, which leads to shorter C–C bond lengths connected to the  $\alpha$ -H (Table 1n and Fig. 4c) and an increased distance between the C–O single bond and the carbonyl group (Table 1l and Fig. 4c). The addition of the Lewis base remotely interacts with the hydrogen atoms of the  $\alpha$ -H in PLA, promoting the formation of enol intermediates (Table 1b, i and Fig. 4d). Extending the length of the branched bond attached to the cation of a straight-chain organic base or reducing the radii of both cations and anions enhances the process of deprotonation.

**3.1.6 Solvation effect of PO.** During PLA transesterification, oxygen anions generated by the reaction between PPNCl and PO maintain their affinity towards proximal hydrogen atoms. The chain propagation of anionic polymerization is closely related to the looseness of ion pairs, with solvation in polar solvents playing a pivotal role in the ion morphology of the active center.<sup>53</sup> Therefore, the accelerated transesterification of PLA in PO can be attributed to both PO as a reactant and the solvation effect imparted by PO as a polar solvent (Fig. S8, S9 and S16†). This influence is also evident in the calculations presented herein. Considering the solvation effect, using PO as the solvent significantly increases the anion–cation distance thereby enhancing the looseness of ion pairs. Furthermore, the distance between the anion and carbonyl group decreases with PO as the solvent (Table 1c and d). The inclusion of PO substantially boosts the depolymerization and transesterification efficiencies of PLA, resulting in a system more prone to nucleophilic substitution reactions.

In summary, analyzing the <sup>1</sup>H NMR chemical shift of  $\alpha$ -H aids in predicting and identifying concurrent transesterification and copolymerization processes. Transesterification of PLA will not occur if Lewis bases fail to induce changes in the chemical shift of specific  $\alpha$ -H sites. Lewis bases capable of modifying the  $\alpha$ -H chemical shift in PLA are considered viable candidates. Adding only Lewis bases results in PLA depolymerization, whereas the integration of Lewis acid–base pairs leads to the production of copolymers. The extent of PLA depolymerization and transesterification is intimately related to the ionic distance between Lewis bases and  $\alpha$ -H of PLA. Anions in the initiator, positioned in close proximity to the  $\alpha$ -H of PLA, facilitate copolymer formation due to deprotonation, leading to modifications in the bond lengths of ester groups. As a polar solvent and an active epoxide, PO has the potential to cause depolymerization and transesterification in PLA.

### 3.2 Initiator activity for both PO/PA/CO<sub>2</sub> copolymerization and PLA transesterification

The Lewis bases mentioned earlier were utilized in the study of ROCOP-T. The PPC-P-co-PLA multi-block copolymers were identified using the notation provided in Fig. 5. When com-



**Fig. 5** (a) Schematic diagram of ROCOP of PO, PA and CO<sub>2</sub> in conjunction with the transesterification of PLA (ROCOP-T). DOSY spectra of products prepared by PO/PA/CO<sub>2</sub> copolymerization and PLA transesterification with TEB and (b) TEA, (c) DBU, (d) TBD, (e) TEBAC, (f) TPACl, (g) TBACl, (h) TPNAC, (i) TEABr, (j) TBPC, (k) BPP, (l) TTPP, and (m) PPnCl as the catalytic system.

bined with TEB, the catalytic system consisting of TPACl, TBACl, TPNAC, BPP, TTPP, and PPnCl enabled the conversion of PLA into PPC-P-*co*-PLA multiblock copolymers *via* transesterification within 6 h. Under identical conditions, using DBU, TEBAC, and TBPC as initiators resulted in only partial conversion of PLA, resulting in PPC-P-*co*-PLA/PLA blends. When TBD was used as the initiator, PE-*co*-PLA copolymers were obtained without chain propagation of CO<sub>2</sub>. TEA and TEABr were ineffective in initiating the transesterification of PLA, leading solely to the production of PPC-P. U1 and DMAP exhibited no activity towards ROCOP of PA, PO, and CO<sub>2</sub>, resulting in no formation of CO<sub>2</sub>-based polymers.

Amidine, a nitrogen-rich organic compound, exhibits stronger alkalinity than amines and has the ability to form stable

salts with acids.<sup>48,54</sup> With DBU serving as the initiator, PPC-P-*co*-PLA multiblock copolymers with a highly regular composition and minimal PPO content were synthesized (Fig. 3e). This was achieved due to DBU's ability to effectively minimize side reactions arising from the nucleophilic nature of bases. PPC-P-*co*-PLA/PLA blends were obtained using DBU as the initiator, given the presence of some unreacted PLA during the same reaction time. In contrast, TBD resulted in the production of PE-*co*-PLA copolymers. TBD significantly influenced the depolymerization of PLA. During the same time frame, incomplete conversion of PA and absence of CO<sub>2</sub> chain propagation were observed (Fig. 5d). When compared to its effects on the depolymerization and transesterification of PLA, TBD demonstrated reduced activity in catalyzing the ROCOP of PO,

PA, and CO<sub>2</sub>. Consequently, with TBD as the initiator, PLA transesterification preceded the chain propagation reactions of PE and PPC. The pK<sub>a</sub> value of TBD surpasses that of DBU,<sup>52</sup> suggesting that higher alkalinity does not inherently correlate with superior performance in copolymerization and PLA transesterification reactions.

Organic ammonium chloride exhibits a regular effect on ROCOP-T. As the carbon chain length on the positive ion of the initiator increased, the molecular weight and the PPC content of the resulting product gradually increased: TPNAC (58.2 kDa, 49.1%) > TBACl (53.7 kDa, 48.6%) > TPACl (39.1 kDa, 46.5%) (entries 9–11, Table 2). This suggests a positive correlation between the increasing carbon chain length ( $\leq 5$ ) of the initiator and the PPC content, which enhances the efficient insertion of CO<sub>2</sub> into the polymer chain, thereby promoting the chain propagation of PPC. The similarity in molecular weight and composition of the products initiated by TBACl and TPNAC suggests that the impact plateaus once the carbon chain length reaches a certain level for initiating ROCOP-T. Compared to TBACl, TPNAC leads to an elevated PPO content in PPC-P-co-PLA multi-block copolymers, likely due to the increased ion looseness. Upon substitution of bromide ions for chloride ions, TBABr, as the initiator for copolymerization and transesterification, results in minimal ester exchange within PLA, yielding PPC-P/PLA blends as the final product. Using TBPC as the initiator yielded PPC-P-co-PLA/PLA blends with a 91.4% conversion rate of PA. TBPC exhibits lower initiation efficiency than TBACl for ROCOP-T. When the carbon chain lengths are equal, the initiation efficiency for ROCOP-T follows the order: TBACl > TBPC > TBABr.

All four currently utilized organic phosphine salts exhibit initiator activity in ROCOP-T. Analysis of the molecular weights of the obtained products indicates a specific activity order of PPnCl > TTPP  $\approx$  BPP > TBPC within the reaction system (entries 13–16, Table 2). When three linear carbon chains of TBPC were substituted with phenyl groups, BPP exhibited increased efficiency in ROCOP-T. However, when all straight-chain carbon chains of TBPC were substituted with phenyl groups, the PPC content in the copolymer composition decreased, impeding the subsequent incorporation of carbon dioxide. In comparison with TTPP, the anions in PPnCl led to enhanced hydrogen delocalization,<sup>41</sup> making it a more efficient Lewis base for ROCOP-T. Among the ionic initiators suitable for ROCOP-T, TBACl, TPNCl and PPnCl were found to be the most efficacious. PPnCl exhibited the highest efficiency in enhancing the insertion of CO<sub>2</sub> into the chain, yielding PPC-P-co-PLA multi-block copolymers with the highest PPC content. Consequently, among the tested ionic initiators, PPnCl emerges as the preferred choice for ROCOP-T.

The formation of PPC-P-co-PLA multi-block copolymers necessitates a balance between the copolymerization reaction rate and the rates of PLA depolymerization and transesterification. In the entire initiator research system, the listed initiators exhibit activity for ROCOP-T, with their efficiency ranked as follows: PPnCl > TPNAC > TBACl > TTPP  $\approx$  BPP > TPACl >

TEBAC > TBPC > DBU. PPnCl was selected as the initiator for further experiments.

### 3.3 Reaction process to synthesize PPC-P-co-PLA multi-block copolymers

To monitor the reaction process, samples were collected at various time points and analysed using <sup>1</sup>H NMR spectra, <sup>13</sup>C NMR spectra, GPC, and FT-IR spectrum (Fig. 6a–d). DOSY spectra were used to differentiate between the obtained PPC-P-co-PLA copolymer and PPC-P/PLA blends (Fig. 6e–g). The schematic illustrates the sequential process of monomer reduction, PPC-P chain extension, and subsequent transesterification reactions between PPC-P and PLA during the reaction (Fig. 6h–j).

The copolymerization of PO, PA, and CO<sub>2</sub> is the key process during the 2 h reaction to produce PPC-P. After 2 h of reaction, residual PA peaks persisted, with a conversion rate to PE of 86.4%, suggesting significant unreacted PA (Fig. 6a). Initially, the concentrations of cyclic carbonate and PPO were low (entry 1, Table S1†). At this stage, the majority of PPC-P polymer chain segments in the system was evident (Fig. 6e). The prominent antisymmetric stretching vibration peak of COC ( $\nu_{\text{as}} \text{COC}$ ) at 1185 cm<sup>-1</sup> indicates the presence of unreacted PLA (Fig. 6d). Notably, a substantial proportion of PLA remained unreacted at this stage. The unreacted PLA may experience fragmentation and shortening due to interactions with Lewis bases (Fig. 6e). Consequently, PPC-P/PLA blends emerged as the primary products during this phase. Analysis of the <sup>13</sup>C NMR spectra (Fig. 6b) indicates that PLA exhibited isotactic stereoisomerism.<sup>55</sup> After 2 h of reaction, the carbonyl peak shape in <sup>13</sup>C NMR remained unchanged, suggesting that transesterification does not affect the stereoisomeric regularity of PLA (Fig. 6b).

After 4 hours of reaction, the primary products obtained were PPC-P-co-PLA/PLA blends (Fig. 6f). The main reactions were ROCOP of PO, PA, and CO<sub>2</sub> to form PPC-P, accompanied by transesterification between PPC-P and PLA to yield PPC-P-co-PLA multi-block copolymers. After 4 h, PA was fully converted to PE (Fig. 6a), resulting in an increase in molecular weight to 46.0 kg mol<sup>-1</sup> (entry 2, Table S1†). Following the complete conversion of PA, the PPC content in the polymer segments increased with consistent CO<sub>2</sub> injection, accompanied by an increase in cyclic carbonate (CC) content due to back-biting. Consequently, the PE content decreased, whereas the PPC and CC contents increased. PLA long chains, which have undergone depolymerization with Lewis bases and activation *via* Lewis acid–base pairs, are continuously linked to PPC-P segments *via* transesterification, resulting in the formation of block copolymers. The notable reduction of the  $\nu_{\text{as}} \text{COC}$  peak at 1185 cm<sup>-1</sup> suggests alterations in the stretching vibration of PLA, which can be attributed to depolymerization and transesterification (Fig. 6d). At this stage, it is noted that some PLA segments in the system have not undergone transesterification to form block copolymers (Fig. 6f).

After 6 hours of reaction, transesterification successfully converted all PLA into PPC-P-co-PLA multi-block copolymers (Fig. 6g). The molecular weight of the PPC-P-co-PLA multi-

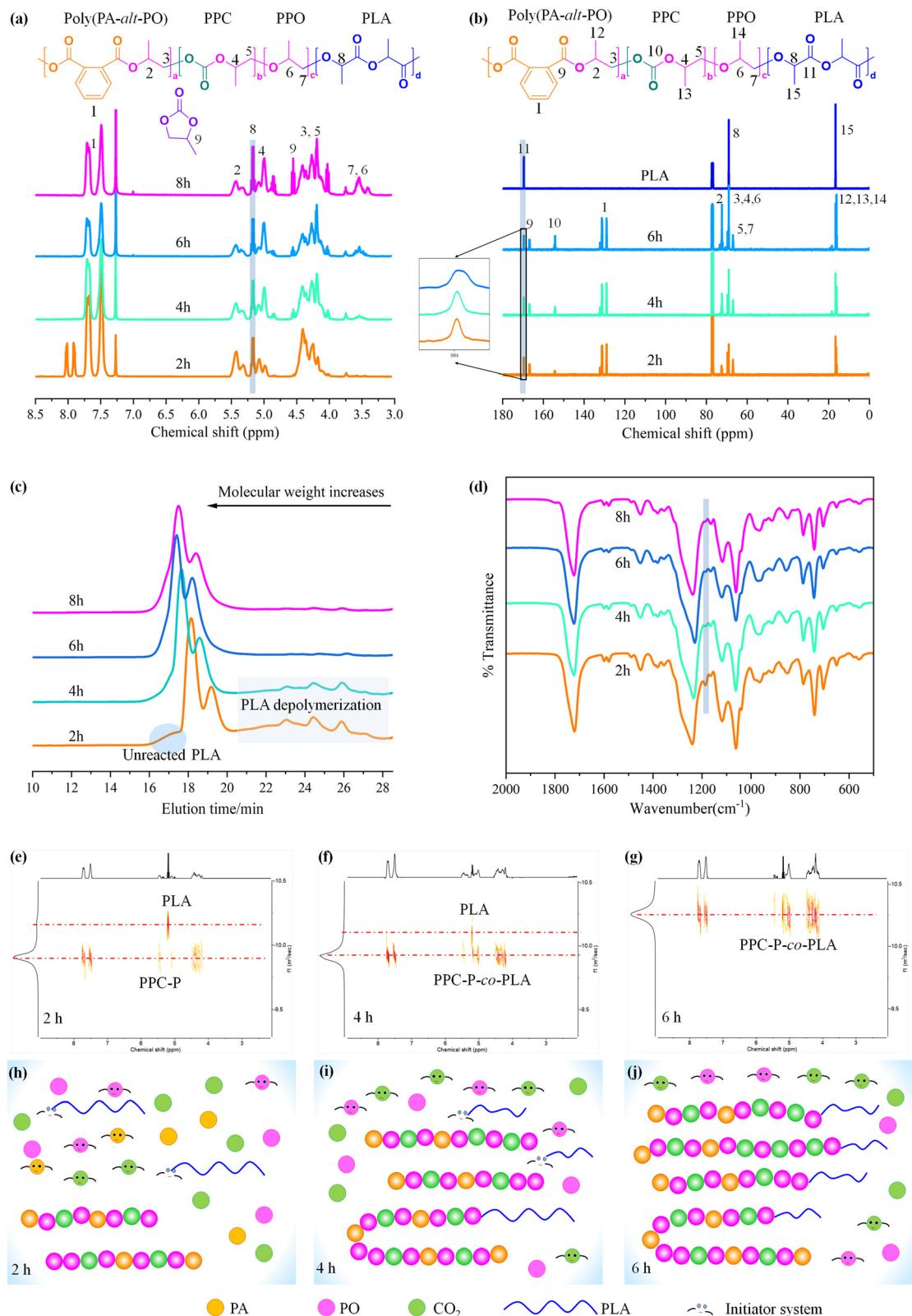


**Fig. 6** (a)  $^1\text{H}$  NMR spectra, (b)  $^{13}\text{C}$  NMR spectra, (c) GPC curves and (d) FT-IR spectrum of the products obtained at various time points using a reactant ratio of PO : PA : TEB : PPNCI 4000 : 500 : 2 : 1, the amount of PLA being 10 wt%, and the  $\text{CO}_2$  pressure below 1 Megapascal. DOSY spectra of the resultant PO/PA/ $\text{CO}_2$ /PLA obtained after reaction durations of 2 h (e), 4 h (f) and 6 h (g). Schematic diagrams illustrating the compositional evolution of the reaction system at reaction times of 2 h (h), 4 h (i) and 6 h (j).

block copolymers was determined to be  $48.4 \text{ kg mol}^{-1}$  (entry 3, Table S1†). The increase in molecular weight was insignificant when compared to the 4-hour reaction. Consequently, transesterification of PLA remained the dominant reaction throughout, with continuous introduction of  $\text{CO}_2$ . The carbonyl peak corresponding to the 6 h product showed a broadened profile in the  $^{13}\text{C}$  NMR spectra. The broadening is presumably attributed to changes in the chemical environment of PLA following transesterification to PPC-P-co-PLA, despite the carbonyl peak retaining its singlet nature. As an active anion reaction, the continuous addition of  $\text{CO}_2$  occurs when chain termination is absent. The side effects associated with the back-biting reaction increased substantially, resulting in a concurrent rise in CC levels (entry 4, Table S1†). Hence, precise control of reaction time and conditions is crucial for the successful outcome of this reaction. 6 h was identified as the optimal reaction time with PPNCl as the initiator, which was maintained for all subsequent reactions.

### 3.4 Competitive polymerization rate and reaction mechanism

PPC-P-co-PLA multi-block copolymers were synthesized *via* ROCOP-T, incorporating PE derived from PA, PPC generated from  $\text{CO}_2$ , a minor quantity of PPO, and PLA through transesterification. As the content of TEB increased, the interaction between TEB and PO intensified, leading to an enhanced PPO concentration and a corresponding decrease in PPC. The enhanced binding of TEB with Lewis bases simultaneously reduced the affinity of the Lewis base for PLA, mitigating PLA depolymerization into oligomers and ultimately increasing PLA content (Fig. 7a). From a holistic perspective, it is notable that despite using more reaction materials compared to ROCOP of PO, PA, and  $\text{CO}_2$ , a TEB molar ratio of 2.0 adequately fulfills the experimental prerequisites for copolymerization and PLA transesterification. Upon maintaining a constant molar ratio of PA, an elevation in PO content resulted in a corresponding increase in PPC content, while PE content decreased significantly and PLA content exhibited a slight decrease (Fig. 7b). At a constant molar ratio of PO, an increase in PA content led to an elevation in PE content, a reduction in PPC content, and minimal changes in PLA content (Fig. 7c). The PE and PPC contents are closely related to the PO/PA ratio. PA has the highest reaction rate, slightly surpassing  $\text{CO}_2$ . After the termination of PA chain propagation, the continuous chain growth with  $\text{CO}_2$  proceeds to produce the random copolymer PPC-P.<sup>26,27</sup> Altering the feeding ratio modifies the structure of PPC-P. When the PO:PA ratio is adjusted from 3000:400 to 3000:250, there is a notable increase in PO/ $\text{CO}_2$  chain segments in PPC (Fig. S17†). The presence of PA has little effect on the depolymerization and transesterification of PLA. With a constant PO:PA ratio, an increase in copolymer raw material content led to an increase in PE content and a corresponding decrease in PPC, PPO, and PLA content (entries 8 and 9, Table 3). An increase in PLA content resulted in a continuous decrease in the PPC mole fraction, suggesting a decrease in  $\text{CO}_2$  conversion, while PE mole content remained stable, suggesting unaffected PA conversion (Fig. 7d). At a PLA

mass fraction of 16%, some PLA molecules were not fully ester-exchanged with PPC-P, resulting in the formation of PPC-P-co-PLA/PLA blends (Fig. S18†). PLA segments are covalently attached to the PPC termini within PPC-P, serving as end-capping agents through anion transfer (Fig. S19†). Consequently, the resultant block copolymer consists of random PPC-P and depolymerized PLA by transesterification. Furthermore, increased PLA content suppresses  $\text{CO}_2$  chain growth, resulting in shorter PPC-P segments and a subsequent decrease in the PPC-P-co-PLA copolymer molecular weight.

The copolymerization reaction rate between PA and  $\text{CO}_2$  exhibits insignificant variation ( $K_2 \approx K_1$ ) and resembles that of PLA depolymerization catalysed by PPNCl ( $K_1 \approx K_3$ ). Competitive insertion of PA and  $\text{CO}_2$  results in the formation of carboxylate and carbonate species. Subsequently, the insertion of PO into these species yields alkoxide intermediates.<sup>26</sup> During chain propagation, carboxylate exhibits the fastest chain extension and remains relatively unaffected by PLA ( $K_5 > K_4$ ). PLA transesterification and  $\text{CO}_2$  chain growth compete, with  $\text{CO}_2$  chain propagation closely approaching the equilibrium constant of PLA transesterification ( $K_4 \approx K_6$ ). Transesterification between PPC-P and PLA terminates one end of PPC-P with PLA. The proposed reaction mechanism is depicted in Fig. 7e. The released initiator system undergoes nucleophilic substitution reactions with PLA in PPC-P-PLA copolymers, leading to the formation of shorter PLA segments. The newly formed shorter PLA segments with active ends will undergo further transesterification with PPC segments in PPC-P. Continuous transesterification reactions ultimately yield multi-block copolymers with similar PLA chain lengths (Fig. 7f). If the initiator remains active, the continuous reaction will result in PLA segments in the copolymers of similar length to those obtained in the corresponding proportion in Fig. 1c.

### 3.5 Thermal properties and crystallinity of PPC-P-co-PLA multi-block copolymers

Thermogravimetric analysis (TGA) and differential scanning calorimetry (DSC) measurements were conducted to assess the thermal behavior of the copolymers. When compared to PPC-P, the  $T_{5\%}$  of the copolymer increased by 18 to 45 °C (Fig. 8a), indicating that the incorporation of PLA enhances the overall structural stability of the copolymer. At a PLA mass fraction of 12 wt%, the copolymer achieved a maximum  $T_{5\%}$  value of 280.4 °C. The DTG curves, derived from the thermogravimetric curve through differentiation, provide insights into the rate of weight loss. The decomposition of the PPC-P-co-PLA multi-block copolymers occurs in two distinct stages (Fig. 8b). With increasing PLA content, the decomposition temperature of the PPC chain segment in the first stage consistently increases. This implies an enhancement in the thermal decomposition resistance of the chain segment, due to interactions between PLA and one terminus of PPC (Fig. S18†). Consequently, an increase in PLA content results in enhanced thermal stability of the copolymer.



**Fig. 7** Compositional variation charts of PPC-P-co-PLA multi-block copolymers by varying the molar ratios of TEB (a), PO (b), and PA (c), as well as adjusting the PLA content (d). The data utilized for creating the charts originated from the following entries in Table S4:† (a) entries 1–4; (b) entries 5, 6, 1 and 7–11; (c) entries 3 and 11–15. (e) Proposed reaction mechanism of PO, PA, and CO<sub>2</sub> copolymerization and PLA transesterification. (f) Proposed reaction mechanism for generating multi-block copolymers through continuous transesterification.

The PPC-P-co-PLA multi-block copolymers synthesized *via* ROCOP-T exhibit crystalline domains, qualifying them as semi-crystalline copolymers (Fig. 8d and e). DSC analysis of the PPC-P-co-PLA multi-block copolymers revealed two crystalliza-

tion melting peaks at a PLA content of approximately 4 wt%. When the PLA mass fraction was increased to 8 wt%, two crystallization melting peaks emerged during the first heating cycle, while only one peak persisted during the second cycle.

**Table 3** PO, PA, and CO<sub>2</sub> copolymerization and PLA transesterification by compositional variation

Entry	PO/PA/TEB/PPNCl	PO/PA	PE <sup>a</sup> (%)	PPC <sup>a</sup> (%)	PPO <sup>a</sup> (%)	PLA <sup>a</sup> (%)	CC <sup>a</sup> (%)	PLA <sup>a</sup> (wt%)	CO <sub>2</sub> <sup>a</sup> (wt%)	M <sub>n</sub> <sup>b</sup> (kg mol <sup>-1</sup> )	PDI <sup>b</sup>
1	3000 : 250 : 1.6 : 1	12	19.7	66.7	3.3	10.3	8.2	6.3	24.9	33.7	1.58
2	3000 : 250 : 1.8 : 1	12	21.7	58.7	7.6	12.0	7.5	7.3	22.0	37.6	1.51
3	3000 : 250 : 2.0 : 1	12	20.9	59.8	7.4	11.9	7.8	7.3	22.5	37.6	1.53
4	3000 : 250 : 2.2 : 1	12	23.5	53.6	10.3	12.5	9.1	7.6	20.0	32.5	1.58
5	4000 : 250 : 2.0 : 1	16	14.2	70.6	7.1	8.1	4.5	5.2	27.9	53.1	1.54
6	3500 : 250 : 2.0 : 1	14	17.7	66.7	5.9	9.8	7.9	6.1	25.5	42.8	1.43
7	2500 : 250 : 2.0 : 1	10	21.1	58.2	9.8	10.9	9.0	6.7	22.0	42.8	1.58
8	2000 : 250 : 2.0 : 1	8	23.1	55.4	10.3	11.2	6.4	6.8	20.6	31.9	1.46
9	4000 : 500 : 2.0 : 1	8	33.6	52.4	4.2	9.9	5.3	5.4	17.4	48.8	1.38
10	3500 : 500 : 2.0 : 1	7	35.4	49.9	4.7	10.1	4.5	5.4	16.4	48.0	1.37
11	3000 : 500 : 2.0 : 1	6	38.7	42.3	7.8	11.1	5.7	5.9	13.7	36.0	1.47
12	3000 : 450 : 2.0 : 1	6.7	31.9	49.9	8.1	10.0	6.3	5.6	17.1	42.6	1.51
13	3000 : 400 : 2.0 : 1	7.5	30.9	51.4	7.1	10.6	4.7	6.0	17.7	38.0	1.46
14	3000 : 350 : 2.0 : 1	8.6	27.2	54.1	8.6	10.1	6.7	5.9	19.3	37.5	1.47
15	3000 : 300 : 2.0 : 1	10	24.8	55.2	10.3	11.8	4.8	7.0	19.9	42.8	1.58
16	4000 : 500 : 2.0 : 1	8	34.0	62.5	3.4	0.0	7.4	0.0	20.2	74.3	1.47
17	4000 : 500 : 2.0 : 1	8	31.1	58.3	6.6	4.0	6.3	2.2	19.7	67.3	1.46
18	4000 : 500 : 2.0 : 1	8	34.0	53.9	3.9	8.2	6.0	4.3	19.2	61.8	1.44
19	4000 : 500 : 2.0 : 1	8	33.8	46.8	4.6	14.8	3.9	8.2	15.8	55.7	1.34
20	4000 : 500 : 2.0 : 1	8	33.2	36.7	8.8	21.2	3.1	12.1	12.8	42.2	1.36
21	4000 : 500 : 2.0 : 1	8	33.5	30.7	8.1	27.7	3.9	16.0	10.8	35.5	1.39
22	4000 : 500 : 2.0 : 1	8	31.4	30.7	5.9	32.0	5.5	18.8	11.0	38.3	1.46

<sup>a</sup> Calculated by <sup>1</sup>H NMR; PE% =  $A_1/4/(A_1/4 + A_4 + (A_{6,7})/3 + A_8) \times 100$ ; PPC% =  $A_4/(A_1/4 + A_4 + (A_{6,7})/3 + A_8) \times 100$ ; PPO% =  $(A_{6,7})/3/(A_1/4 + A_4 + (A_{6,7})/3 + A_8) \times 100$ ; PLA% =  $A_8/(A_1/4 + A_4 + (A_{6,7})/3 + A_8 + A_c) \times 100$ ; CC% =  $A_9/(A_2 + A_4 + (A_{6,7})/3 + A_8 + A_c) \times 100$ ; PLAw% =  $72 \times \text{PLA}\% / (72 \times \text{PLA}\% + 206 \times \text{PE}\% + 102 \times \text{PPC}\% + 58 \times \text{PPO}\%) \times 100$ ; CO<sub>2</sub>w% =  $44 \times \text{PPC}\% / (72 \times \text{PLA}\% + 206 \times \text{PE}\% + 102 \times \text{PPC}\% + 58 \times \text{PPO}\%) \times 100$ . <sup>b</sup> Determined by GPC in tetrahydrofuran (THF).

At a PLA mass fraction of 12 wt%, a single crystallization melting peak was observed during the first heating cycle, reaching a maximum temperature of 164.6 °C. When the PLA mass fraction reached 16 wt%, both the crystallization melting peak and the thermal decomposition temperature decreased. The decrease could be attributed to PLA acting as a capping agent, which hindered the incorporation of CO<sub>2</sub>, resulting in reduced copolymer molecular weight and incomplete attachment of PLA to PPC-P during copolymer formation. The DSC second heating curve showed that the incorporation of PLA increased the glass transition temperature (*T*<sub>g</sub>) of the PPC-P-co-PLA multiblock copolymers to above 47.9 °C, exhibiting distinct relaxation peaks (Fig. 8e). At a PLA mass fraction of 12 wt%, the *T*<sub>g</sub> of PPC-P-co-PLA multi-block copolymers increased to 49.2 °C, expanding the potential applications. An increase in the PLA mass fraction leads to the expansion of crystalline domains within the copolymer, consequently reducing its transmittance. The transmittance of PPC-P-co-PLA multi-block copolymers consistently exceeded 80% when the PLA content in the polymer remained below 16 wt% (Table S2†).

The crystallinity of the PLA segments was calculated using DSC curves and the crystallinity of the overall copolymer was determined using XRD patterns (Fig. 8f). Crystallinity from the DSC curves was calculated based on the endothermic enthalpy of a single crystallization melting peak and the exothermic enthalpy related to cold crystallization during the initial heating cycle. A gradual increase in crystallinity was observed with an increasing mass fraction of PLA (Table S2†). In essence, an increase in PLA content corresponds to an increase

in crystalline regions within the copolymer. The commercial high-modulus PLA used after drying exhibits an exceptionally high crystallinity of ~99.5%. At a mass fraction of 12.1 wt%, the crystallinity is 63.0%. This indicates that over 60% of the PLA segments in the copolymer have effectively crystallized. XRD analysis reveals that the PLA employed exhibits a fully amorphous structure, encompassing five distinct crystal forms. The diffraction peaks are observed at 2θ values of 14.8°, 16.6°, 18.9°, 22.3°, and 28.8° correspond to the (010), (200/100), (203), (105), and (018) lattice planes, respectively.<sup>55–57</sup> At a concentration of 4 wt% PLA, a distinct peak appears at 16.6°, indicating the subsequent formation of a crystalline region within the copolymer. Increasing the PLA content in the copolymer to 12 wt% leads to a pronounced and distinct 2θ peak at 16.6° in the XRD pattern. The relative crystallinity is calculated as the ratio of the crystallization peak area to the total area in the XRD pattern. To analyse the proportion of the crystalline region within the copolymer, we examined the XRD pattern of PLA containing 12 wt% and determined a crystallinity of 12.3% using integral area calculations.

### 3.6 Mechanical and rheological properties of PPC-P-co-PLA multi-block copolymers

Mechanical performance testing revealed that PPC-P, composed of 34% PE and having a molecular weight of 74.3 kg mol<sup>-1</sup>, exhibited a tensile strength of 44.5 ± 0.4 MPa and an elongation at break of 6.6 ± 1.8%. The incorporation of 4 wt% PLA into PPC-P-co-PLA multiblock copolymers resulted in a slight decrease in tensile strength to 42.3 ± 0.6 MPa. Increasing the PLA content to 8 wt% led to enhancement of



**Fig. 8** (a) TGA curves and (b) DTG curves of PPC-P-co-PLA multi-block copolymers with different mass fractions of PLA. (c) Changes in  $T_g$ ,  $T_m$  and  $T_{5\%}$  of PPC-P-co-PLA multi-block copolymers with different mass fractions of PLA. DSC curves of PPC-P-co-PLA multi-block copolymers with different mass fractions of PLA: (d) first heating run at  $10\text{ }^\circ\text{C min}^{-1}$ ; (e) second heating run at  $10\text{ }^\circ\text{C min}^{-1}$ . (f) XRD patterns of PLA and PPC-P-co-PLA multi-block copolymers with different mass fractions of PLA.



**Fig. 9** (a) Stress–strain curves, (b) storage modulus  $G'$ , (c) loss modulus  $G''$  and (d) complex viscosity  $\eta^*$  of PPC-P-co-PLA multi-block copolymers with different mass fractions of PLA.

the tensile strength to  $46.3 \pm 0.9$  MPa and elongation at break to  $8.3 \pm 1.6\%$ . The percentage content of each component in this copolymer PE/PPC/PPO/PLA was 34/47/4/15. By calculating the number of each repeating unit within the polymer, the composition was as follows: PE 92, PPC 257, PPO 38, and PLA 116. At a PLA content of 12 wt%, the PE content remained stable, while the PPC content decreased by 10%. The material exhibited brittle fracture and minimal deformation, potentially due to a decrease in molecular weight.

Rheological testing reveals that changes in storage modulus  $G'$ , loss modulus  $G''$  and complex viscosity  $\eta^*$  as the PLA content increases mirrored those observed in tensile strength. Complex viscosity ( $\eta^*$ ) encapsulates both elastic and viscous characteristics of the material. Analysis of composite viscosity revealed a decrease followed by an increase when the PLA content was 4 wt%. The initial decrease was attributed to the rheological properties of PPC-P, whereas the subsequent increase was likely due to PLA crystallization. When the PLA content reached 8 wt%, a substantial rise in the composite material's viscosity was observed as the angular frequency increased from 1 to 10  $\text{rad s}^{-1}$ . During tensile hardening of plastics, changes in molecular chain orientation and crystallinity enhance the material's elasticity, with the elastic modulus typically increasing as a result of strain or time. As the tensile strain intensifies, molecular chain orientation and entanglement become more pronounced, enhancing the material's resistance to flow and, consequently, increasing complex viscosity. The phenomenon diminished as the PLA content further increased. Based on their mechanical and rheological properties, copolymers with a PLA content of 4–8 wt% showed superior performance compared to those with 12–16 wt% PLA. Among them, copolymers containing 8 wt% PLA exhibited the best performance and had the highest application potential (Fig. 9).

## 4. Conclusions

Semi-crystalline PPC-P-co-PLA multi-block copolymers were successfully synthesized using ROCOP of PO, PA and CO<sub>2</sub> in conjunction with the transesterification of PLA *via* a one pot/one-step method. The sole addition of Lewis bases leads to the depolymerization of PLA, whereas Lewis acid–base pairs as catalysts promote the formation of copolymers. Lewis bases capable of inducing changes in the  $\alpha$ -H chemical shift of PLA, which can be further altered by the addition of TEB, are suitable for concurrent transesterification and copolymerization processes. The depolymerization and transesterification of PLA are closely related to the degree of ion pair loosening, deprotonation and solvation effects. For the ROCOP-T process, the sequence of initiator activity is as follows: PPNCI > TPNAC > TBACl > TTPP  $\approx$  BPP > TPACl > TEBAC > TBPC > DBU. TEB/PPNCI shows the highest catalytic activity in the synthesis of the semi-crystalline copolymer. Initially, PPC-P is formed, followed by transesterification with PLA to yield PPC-P-co-PLA multi-block copolymers. The copolymer containing 12 wt%

PLA exhibits optimal thermal performance, with a thermal decomposition temperature of 280.4 °C, a maximum crystallization melting temperature of 164.6 °C, and a glass transition temperature of 49.2 °C. The crystallinity of PLA in the PPC-P-co-PLA copolymer with 12 wt% PLA reaches 63%, and the overall crystallinity of the copolymer is 12%. Copolymers containing 8 wt% PLA demonstrated superior performance, with a tensile strength of  $46.3 \pm 0.9$  MPa and an elongation at break of  $8.3 \pm 1.6\%$ . This research significantly enhanced the chemical utilization efficiency of carbon dioxide and, meanwhile, offers a novel perspective on the sustainable reuse of polyesters and the synthesis of semi-crystalline copolymers.

## Data availability

The data supporting this article have been included as part of the ESI.†

## Conflicts of interest

The authors declare that they have no known competing financial interests or personal relationships that could have appeared to influence the work reported in this paper.

## Acknowledgements

Financial support was provided by the Fundamental Research Fund of Henan Academy of Sciences (230603001 & No. 240618065), High-level Talent Research Start-up Project Funding of Henan Academy of Sciences (232018002 & No. 241818084), the Scientific and Technological Research Project of Henan Academy of Sciences (242102230180), Joint Fund of Henan Province Science and Technology R&D Program (235200810027), Research and Development Project of Henan Academy of Science (241603011 & 231818020), Henan Provincial Natural Science Foundation General Project (242300420193), the National Natural Science Foundation of China (No. 22075254), and the International Science and Technology Cooperation Project of Henan Province (242102521042). We also appreciate the financial supports from industries: Shandong Lecron Industrial Development Group, Co., Ltd, China, Zhuhai Zhongguan Petrochemical, Co., Ltd, China, Guangdong Tianxin New Material Technology Co., Ltd, China, Hebei CNC Risun Energy Co., Ltd, China, and Huanghua Xinnuolixing Fine Chemicalstock Co., Ltd, China.

## References

- 1 Y. Xu, L. Lin, M. Xiao, S. Wang, A. T. Smith, L. Sun and Y. Meng, *Prog. Polym. Sci.*, 2018, **80**, 163–182.
- 2 H. Dau, G. R. Jones, E. Tsogtgerel, D. Nguyen, A. Keyes, Y.-S. Liu, H. Rauf, E. Ordonez, V. Puchelle, H. Basbug

- Alhan, C. Zhao and E. Harth, *Chem. Rev.*, 2022, **122**(18), 14471–14553.
- 3 G. Hayes, M. Laurel, D. MacKinnon, T. Zhao, H. A. Houck and C. R. Becer, *Chem. Rev.*, 2022, **123**(5), 2609–2734.
- 4 Z. Zhang, Y. Ren, J. Liang, M. Xiao, S. Wang, S. Huang, D. Han and Y. Meng, *Energy Storage Mater.*, 2024, **71**, 103667.
- 5 S. Inoue, H. Koinuma and T. Tsuruta, *J. Polym. Sci., Part B: Polym. Phys.*, 1969, **7**(4), 287–292.
- 6 Y. Wang and D. J. Darensbourg, *Coord. Chem. Rev.*, 2018, **372**, 85–100.
- 7 T. Ohkawara, K. Suzuki, K. Nakano, S. Mori and K. Nozaki, *J. Am. Chem. Soc.*, 2014, **136**(30), 10728–10735.
- 8 L. Yang, S. Liu, Z. Zhou, R. Zhang, H. Zhou, C. Zhuo and X. Wang, *Macromolecules*, 2023, **57**(1), 150–161.
- 9 L. Tang, M. Xiao, Y. Xu, S. Wang and Y. Meng, *J. Polym. Res.*, 2013, **20**, 190.
- 10 X.-H. Zhang, R.-J. Wei, Y. Y. Zhang, B.-Y. Du and Z.-Q. Fan, *Macromolecules*, 2015, **48**(3), 536–544.
- 11 Q. Wang, X. Li, H. Li, L. Liu, X. Zhang, Y. Li, M. Kang, Q. Li and J. Wang, *J. Environ. Chem. Eng.*, 2025, **13**, 115928.
- 12 C. A. L. Lidston, S. M. Severson, B. A. Abel and G. W. Coates, *ACS Catal.*, 2022, **12**(18), 11037–11070.
- 13 D. J. Darensbourg, R. M. Mackiewicz, J. L. Rodgers, C. C. Fang, D. R. Billodeaux and J. H. Reibenspies, *Inorg. Chem.*, 2004, **43**(19), 6024–6034.
- 14 J. Liu, W. Ren, Y. Liu and X. Lu, *Macromolecules*, 2013, **46**(4), 1343–1349.
- 15 R. Chiarcos, M. Laus, K. Sparnacci, R. Po, P. Biagini, I. Tritto, L. Boggioni and S. Losio, *Eur. Polym. J.*, 2023, **192**, 112058.
- 16 D. Zhang, S. K. Boopathi, N. Hadjichristidis, Y. Gnanou and X. Feng, *J. Am. Chem. Soc.*, 2016, **138**(35), 11117–11120.
- 17 Y.-Y. Zhang, G.-W. Yang, R. Xie, X.-F. Zhu and G.-P. Wu, *J. Am. Chem. Soc.*, 2022, **144**(43), 19896–19909.
- 18 J. Liang, S. Ye, S. Wang, S. Wang, D. Han, S. Huang, Z. Huang, W. Liu, M. Xiao, L. Sun and Y. Meng, *Macromolecules*, 2022, **55**(14), 6120–6130.
- 19 P. Du, Y. Li and X. Lu, *Macromolecules*, 2023, **56**(17), 6783–6789.
- 20 Y. Ren, T. Zhang, S. Wang, D. Han, S. Huang, H. Guo, M. Xiao and Y. Meng, *J. CO<sub>2</sub> Util.*, 2024, **85**, 102853.
- 21 C. Chen, Y. Gnanou and X. Feng, *Polym. Chem.*, 2022, **13**(45), 6312–6321.
- 22 C. Hu, X. Pang and X. Chen, *Macromolecules*, 2022, **55**(6), 1879–1893.
- 23 A. C. Deacy, G. L. Gregory, G. S. Sulley, T. T. D. Chen and C. K. Williams, *J. Am. Chem. Soc.*, 2021, **143**(27), 10021–10040.
- 24 W. Yu, E. Maynard, V. Chiaradia, M. C. Arno and A. P. Dove, *Chem. Rev.*, 2021, **121**(18), 10865–10907.
- 25 S. J. Poland and D. J. Darensbourg, *Green Chem.*, 2017, **19**(21), 4990–5011.
- 26 J. Liang, S. Ye, W. Wang, C. Fan, S. Wang, D. Han, W. Liu, Y. Cui, L. Hao, M. Xiao and Y. Meng, *J. CO<sub>2</sub> Util.*, 2021, **49**, 101558.
- 27 V. K. Chidara, S. K. Boopathi, N. Hadjichristidis, Y. Gnanou and X. Feng, *Macromolecules*, 2021, **54**(6), 2711–2719.
- 28 N. Kawashima, T. Yagi and K. Kojima, *Sustainability*, 2021, **13**(1654), 1–18.
- 29 M. Meng, S. Wang, M. Xiao and Y. Meng, *Sustainable Polym. Energy*, 2023, **1**(1), 1–43.
- 30 H. Li, H. Luo, J. Zhao and G. Zhang, *ACS Macro Lett.*, 2018, **7**(12), 1420–1425.
- 31 H. Kudo, S. Nishioka, H. Jin, H. Maekawa, S. Nakamura and T. Masuda, *Polymer*, 2022, **240**, 124489.
- 32 C. Hu, X. Chen, M. Niu, Q. Zhang, R. Duan and X. Pang, *Macromolecules*, 2022, **55**(2), 652–657.
- 33 J. Liu, M. Jia, Y. Gnanou and X. Feng, *Macromolecules*, 2023, **56**(4), 1615–1624.
- 34 S. Ye, J. Liang, Y. Ren, S. Wang, D. Han, S. Huang, Z. Huang, M. Xiao and Y. Meng, *Sustainable Polym. Energy*, 2023, **1**(1), 1–13.
- 35 S. Schüttner, C. Gardiner, F. S. Petrov, N. Fotaras, J. Preis, G. Floudas and H. Frey, *Macromolecules*, 2023, **56**(20), 8247–8259.
- 36 G. Huang, Y. Zou, M. Xiao, S. Wang, W. Luo, D. Han and Y. Meng, *Polym. Degrad. Stab.*, 2015, **117**, 16–21.
- 37 L. Tang, W. Luo, M. Xiao, S. Wang and Y. Meng, *J. Polym. Sci., Part A: Polym. Chem.*, 2015, **53**(14), 1734–1741.
- 38 X. Li, R.-l. Duan, C.-y. Hu, X. Pang and M.-x. Deng, *Polym. Chem.*, 2021, **12**(11), 1700–1706.
- 39 B. Dong, G. Xu, R. Yang, X. Guo and Q. Wang, *Macromolecules*, 2023, **56**(24), 10143–10152.
- 40 T. M. McGuire, A. Buchard and C. Williams, *J. Am. Chem. Soc.*, 2023, **145**(36), 19840–19848.
- 41 S. H. Dempsey and S. R. Kass, *J. Org. Chem.*, 2022, **87**(22), 15466–15482.
- 42 W. N. Sit, S. M. Ng, K. Y. Kwong and C. P. Lau, *J. Org. Chem.*, 2005, **70**, 8583–8586.
- 43 D. J. Darensbourg, R. M. Mackiewicz, A. L. Phelps and D. R. Billodeaux, *Acc. Chem. Res.*, 2004, **37**, 836–844.
- 44 D. J. Darensbourg and D. R. Billodeaux, *Inorg. Chem.*, 2005, **44**, 1433–1442.
- 45 J. K. Varghese, N. Hadjichristidis, Y. Gnanou and X. Feng, *Polym. Chem.*, 2019, **10**(27), 3764–3771.
- 46 L. Lin, J. Liang, Y. Xu, S. Wang, M. Xiao, L. Sun and Y. Meng, *Green Chem.*, 2019, **21**(9), 2469–2477.
- 47 N. J. Sherck, H. C. Kim and Y.-Y. Won, *Macromolecules*, 2016, **49**(13), 4699–4713.
- 48 H. A. Brown, A. G. De Crisci, J. L. Hedrick and R. M. Waymouth, *ACS Macro Lett.*, 2012, **1**(9), 1113–1115.
- 49 N. Fanjul-Mosteirín, C. Jehanno, F. Ruipérez, H. Sardon and A. P. Dove, *ACS Sustainable Chem. Eng.*, 2019, **7**(12), 10633–10640.
- 50 G. Scoponi, N. Francini, V. Paradiso, R. Donno, A. Gennari, R. d'Arcy, C. Capacchione, A. Athanassiou and N. Tirelli, *Macromolecules*, 2021, **54**(20), 9482–9495.
- 51 T. S. Stukenbroeker, J. S. Bandar, X. Zhang, T. H. Lambert and R. M. Waymouth, *ACS Macro Lett.*, 2015, **4**(8), 853–856.
- 52 M. Hong, J. Chen and E. Y. X. Chen, *Chem. Rev.*, 2018, **118**(20), 10551–10616.

- 53 E. F. de Lima, J. W. de M. Carneiro, C. Fenollar-Ferrer, S. Miertus, S. Zinoviev, N. C. Om Tapanes and D. A. G. Aranda, *Fuel*, 2010, **89**(3), 685–690.
- 54 M. Castillo-Santillan, D. Maniar, M. C. Gutiérrez, P. Quiñonez-Angulo, J. R. Torres-Lubian, K. Loos and J. D. Mota-Morales, *ACS Appl. Polym. Mater.*, 2023, **5**(7), 5110–5121.
- 55 H. Tsuji and Y. Arakawa, *Polym. Chem.*, 2018, **9**(18), 2446–2457.
- 56 Y. Su, Y. Zhao, W. Zheng, H. Yu, Y. Liu and L. Xu, *ACS Appl. Mater. Interfaces*, 2020, **12**(49), 55520–55526.
- 57 Y. Zhang, M. T. Müller, R. Boldt and M. Stommel, *ACS Appl. Polym. Mater.*, 2023, **6**(1), 419–432.